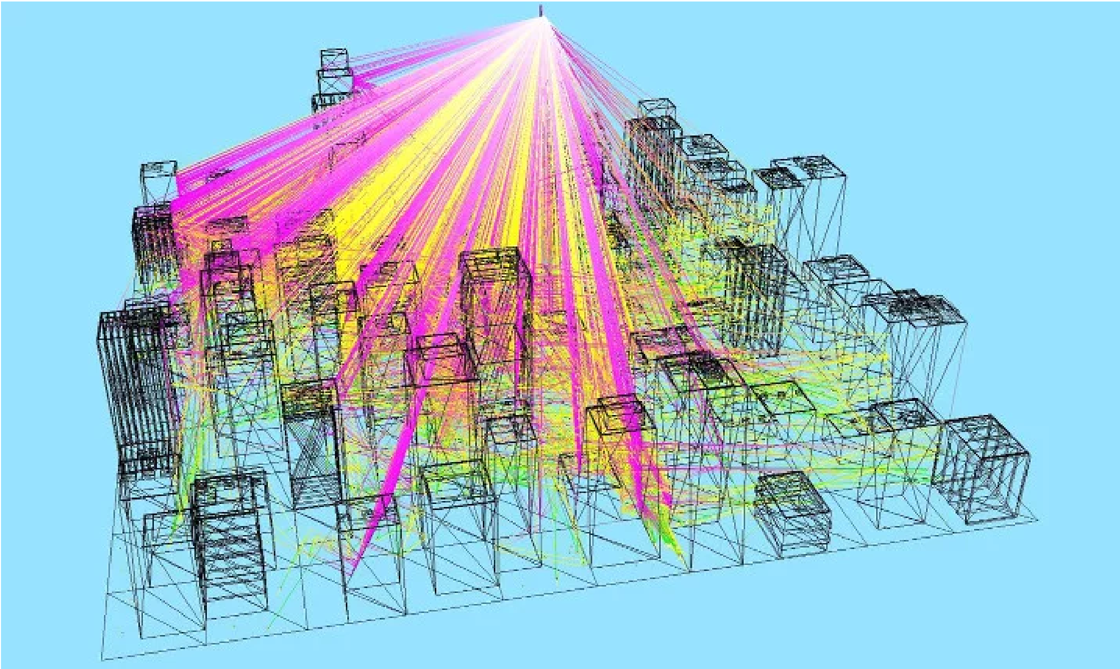

Modeling GNSS Errors in Urban Canyons with Ray Tracing

Master's Thesis in Automotive Engineering

SHIYAO SONG

RUIXUAN JIANG

DEPARTMENT OF ELECTRICAL ENGINEERING

CHALMERS UNIVERSITY OF TECHNOLOGY

Gothenburg, Sweden 2022

www.chalmers.se

Master's thesis 2022

Modeling GNSS Errors in Urban Canyons with Ray Tracing

SHIYAO SONG

RUIXUAN JIANG

Department of Electrical Engineering
Chalmers University of Technology
Gothenburg, Sweden 2022

Modeling GNSS Errors in Urban Canyons with Ray Tracing
SHIYAO SONG
RUIXUAN JIANG

Supervisor: Rubén Calvillo Portales, Volvo Cars
Examiner: Prof. Henk Wymeersch, Electrical Engineering

Master's Thesis 2022
Department of Electrical Engineering
Chalmers University of Technology
SE-412 96 Gothenburg
Telephone +46 31 772 1000

Typeset in LaTeX
Gothenburg, Sweden 2022

Modeling GNSS Errors in Urban Canyons with Ray Tracing
SHIYAO SONG
RUIXUAN JIANG
Department of Electrical Engineering
Chalmers University of Technology

Abstract

Modeling of Global Navigation Satellite Systems (GNSS) is important to the development and verification of the functions of advanced driver-assistance systems (ADAS). For the Hardware-In-the-Loop test, the GNSS system error should be added on the ideal GNSS signal. Therefore, this paper proposes a GNSS error model, especially for multipath error in urban canyons. First, the satellites and scenarios are generated according to the location and street characteristic. After that, we simulate the signal transmission and reflection using ray tracing method. The multipath error is computed at the pseudorange level and the position is estimated using the least squared (LS) method. Finally, the analysis and discussion are made for the proposed model.

Keywords: GNSS, HIL, Monte Carlo, multipath error, ray tracing, signal reflection

Acknowledgements

We would like to express our thanks of gratitude to Chalmers and Volvo Cars for giving us the golden opportunity to do this project. We also want to express our deepest appreciation to our project manager Siddhant Gupta, supervisor Rubén Calvillo Portales as well as our examiner Prof. Henk Wymeersch and advisor Mohammad Farsi who gave us lots of golden advice and help during the thesis work. Beside, we would like to express our special thanks to Russ Whiton from Volvo Cars who kept helping us all the time. In the end, we want to thank all of our families and friends for their encouragement and support throughout the journey.

Shiyao Song & Ruixuan Jiang, Gothenburg, June 2022

List of Acronyms

Below is the list of acronyms that have been used throughout this thesis listed in alphabetical order:

ADAS	advanced driver assistance systems
CADLL	Coupled Amplitude and Delay Lock Loop
CDF	Cumulative Distribution Function
ECEF	Earth-Centered-Earth-Fixed
ECUs	Electronic Control Units
ENU	East-North-Up
GNSS	Global Navigation Satellite Systems
GPS	Global Positioning System
HIL	Hardware In the Loop
IF	Intermediate Frequency
LOS	line-of-sight
LS	Least Square
NLOS	non-line-of-sight
RF	Radio Frequency
TEC	Total Electron Content

Nomenclature

Below is the nomenclature of indices, sets, parameters, and variables that have been used throughout this thesis.

Indices

i	Indices for LS iteration

Parameters & Variables

TEC	Total Electron Content
f	Signal Frequency in Hz
λ	Longitude of the receiver location
ϕ	Latitude of the receiver location
$\mathrm{X_r, Y_r, Z_r}$	Receiver X, Y and Z coordinate in the ECEF system
$\mathrm{x_r, y_r, z_r}$	Receiver x, y and z coordinate in the ENU system
$\mathrm{X_s, Y_s, Z_s}$	Satellite X, Y and Z coordinate in the ECEF system
$\mathrm{x_s, y_s, z_s}$	Satellite x, y and z coordinate in the ENU system
W	Street width in m
H	Building height in m
P	Street width ratio
c	Speed of light in m/s
ϵ	Material relative permittivity
θ_{i}	Signal incidence angle
θ_{e}	Receiver elevation angle in degree
ρ_{f}	Signal power loss coefficient in free space transmission
$\rho_{\perp}$	Perpendicular Fresnel reflection coefficient
$\rho_{\parallel}$	Parallel Fresnel reflection coefficient
ρ_{r}	Signal power loss coefficient due to reflection

P_0	Initial signal power
T_{rate}	Temperature 'laspse' rate
β	Water vapour 'lapse' rate
H_{r}	Altitude of receiver
T	Temperature in K
R_d	Gas constant $287.054 J/Kg/K$
g	Gravity constant 9.80665 m/s^2
$T_{0,\mathrm{dry}}$	Zero-altitude vertical delay terms (dry)
$T_{0,\mathrm{wet}}$	Zero-altitude vertical delay terms (wet)
e_{io}	Ionospheric error
t_{io}	Ionospheric error time delay in s
d	Distance between satellite and receiver in m
e_{m}	Multipath error
L_{d}	Direct signal length
L_{m}	Reflected signal length
L_{c}	Total signal length
L_{t}	True path length between the satellite and receiver
P_{d}	Direct signal power
P_{m}	Reflected signal power
e_{tr}	Troposphere error
PL	Signal power loss
p	Pseudorange between the satellite and the receiver
$e_{\mathrm{x}}, e_{\mathrm{y}}, e_{\mathrm{z}}$	Estimated receiver coordinate error
m	Number of satellite insight.
$\hat{x}, \hat{y}, \hat{z}$	Predicted receiver coordinate

Contents

List of Figures

List of Tables

1
Introduction

In this chapter, the project background, aim, limitation, as well as the ethic issues will be discussed, and the outline structure of the work is presented at the end of this session.

1.1 Background

Advanced driver-assistance systems (ADAS) are of great importance to the automotive industry. And modeling of Global Navigation Satellite Systems (GNSS) has significant potential on the development and verification of ADAS.
Currently, Volvo Car Corporation (VCC) is researching, testing and deploying ADAS functionality in active safety Electronic Control Units (ECUs), which is verified in the Hardware-In-the-Loop (HIL) setup. During the validation and verification process of ADAS functions, the sensor input signals can be simulated for the purpose of cost-saving and efficiency. In the HIL test, some sensor models are already used, such as radar. For GNSS, however, the corresponding models are not sufficiently accurate and representative for functions using satellite signals as inputs, including navigation. The ideal GNSS signal can be generated by the GNSS data simulator GSS7000 from Spirent [1], but the GNSS signal needs to be more realistic. Therefore, how to establish GNSS error model is worthy of investigation.
There are a number of error sources contaminating GNSS signals, such as ionospheric error, tropospheric error, clock offset and multipath error. Among those errors, multipath effect refers to the situation where the satellite signals are reflected before reaching the receiver. In this case, the receiver may view one blurry peak which is biased away from the direct path. Hence, the multipath is responsible for severe errors on the pseudorange and Doppler measurements in certain geographic areas like urban canyons. Also, as the other error models improve, multipath effect becomes a performance bottleneck for lots of applications [2]. Therefore, the modeling of the GNSS multipath error is of great importance.
There are mainly two approaches to model the multipath error: ray tracing model [3] [4] and stochastic model [5]. In the ray tracing model, the GNSS signal transmission and property will be simulated according to the satellite-reflector-antenna geometries. The multipath error is computed due to the simulated GNSS signals. While the stochastic model is generated based on the historical data from the real world experiment. Therefore, it could be more efficient and accurate. However, the stochastic model is highly based on the real data which it is founded on. This means the established stochastic model may not work well when the geometric en-

vironment is different. Compared to the stochastic model, the accuracy of the ray tracing model is limited due to the property of the reflection and the environment complexity. However, the ray tracing model is more appropriate when exploring the signal propagation details and easily portable to new geometric environments[3]. Furthermore, using the ray tracing model, we could adjust the parameters of the model and simulate the very specific scenario. Therefore, we choose the ray tracing method in our study.

The existed multipath models with ray tracing method focus more on the modeling of the building [4], the signal transmission and property [3] and the reception algorithm [6]. But in the HIL verification, we could not only verify ADAS functions in a certain place. Instead, different places around the world need to be simulated to ensure the safety of ADAS functions. This means the real satellite distribution, latitude, longitude of the receiver and the geometry of the street characteristic should be all considered in the multipath error modeling. Furthermore, the signal transmission properties and different signal combinations should be considered to improve the simulated accuracy.

Therefore, a more comprehensive GNSS error model with ray tracing is proposed, which includes the satellite generation, scenario creation, signal simulation through ray tracing, signal reception and position estimation. This model focuses more on generating the real satellite distribution according to the location of the city and creating the real scenario according to the characteristic of the city. In order to improve the simulation accuracy, we use the real satellite distribution for Global Positioning System (GPS) from MATLAB Satellite Communication toolbox with the online ephemeris files. Moreover, the effects of the environment properties and elevation angle on multipath error are explored and analyzed through the proposed model.

1.2 Aim

According to the industry demands and the property of GNSS error, the main task of this thesis work is to explore the possibility of adding the system error on the ideal GNSS data in the domain of HIL simulation. More specifically, the GNSS error from various sources will be modeled, especially the multipath error.

For the multipath model, the modeled multipath error is mainly at the level of pseudorange, the same level as the ideal GNSS signal from the GNSS simulator. During the establishment process of the multipath model, we will combine the latitude, longitude and altitude information of the location, as well as the geometry of street scenarios. In the application of the proposed model in HIL verification, the object location and the geometry should be used as input and the multipath error at the level of pseudorange should be the output. At last, we will explore the possibility to add the generated multipath error on the ideal GNSS signal from simulator.

1.3 Scope/Limitation

The multipath error is heavily related to the geometry of the scenarios and is mainly modeled in this thesis. Since there are already mathematical models for ionospheric error [7], tropospheric error [8] and clock offset, this paper does not focus much on those GNSS errors and will use the existed methods for them.
Another aspect is for the simplification. In the present work, the scenario used to test the error model is simplified, which will be discussed in the following sections. Also for the signal transmission, we only considered about the 1st reflection without multi-reflection or penetration, this is because of the very weak signal power after multi-reflection.
The last thing is that the present thesis focuses on the modeling of the GNSS error at the pseudorange level. And the influence of the receiver's type and property will not be considered.

1.4 Ethical consideration

From the ethical aspect, the research for the GNSS error is mainly conducted in the lab of volvo. There is no risk for the reseacher and no harm to the environment. During the early period of the research, we set up the environment of the GNSS system by connecting the Spirent and HIL setup, which we operate according to the guidelines from Spirent company and volvo.
Also, we obtain the related data and information in a proper and legal way. In order to know the structure of the generated GNSS ideal signal, we check the GNSS generator Spirent, which is approved by volvo. In the error modeling part, we get the real distribution of satellites from the open sources. In the result comparison part, we compare our results with the data from other paper, which is open to the public.

1.5 Outline

This paper is organized as: This Section presents the background, aim and scope of this paper. Section 2 introduces some related theories of GNSS error modeling. And Section 3 presents the methods we use in this thesis for the purpose of GNSS error modeling. The results and discussions of the proposed model are presented in Section 4. Finally, Section 5 summarizes the conclusion, future work and the implications for industrial and academic research.

In summary, to make the HIL simulation closer to the reality, the GNSS error sources need to be modeled. The main challenge is establishing multipath error model. For this part, we introduced two different kind of methods which will be extended in the next sessions.

2

Theory

This chapter mainly introduces the theories of the GNSS error modeling, especially the multipath error, based on the previous research.

2.1 Standard GNSS positioning

GNSS provide the positioning, navigation and timing (PNT), massively used in both civilian and military. In this navigation system, the GNSS receiver will receive the signals from at least four satellites in Medium Earth Orbit (MEO), and then estimate the position through the measurement of the distance that each signal traveled through.
GNSS signals are electromagnetic waves propagating between the satellites and the receiver. One distinct feature of the GNSS signal is the pseudorandom noise (PRN), which is a binary sequence of zeros and ones with no pattern. The receiver will also generate the same PRN code as the GNSS does. Moreover, there will be a time delay between receiver generating the PRN and receiving it from GNSS, and this time delay is the time which the signal travels from GNSS to the receiver. By tracking and continuously comparing the PRN code modulation, the receiver could determine the signal propagation time t. Then, ideally the propagation time could be converted to the traveled distance d by multiplying it with the speed of light c

$$d = \mathrm{ct}. \tag{2.1}$$

After knowing the distance d from Eq(2.1), and the satellite position is also known from the signal information, note as x_0, y_0, z_0, then by assuming the user position as x, y, z, and the receiver clock offset as d_0, then the distance can be expressed as

$$d = \sqrt{(x_0 - x)^2 + (y_0 - y)^2 + (z_0 - z)^2 - d_0} \tag{2.2}$$

.
The Eq(2.2) represents one measurement form one satellite, there are 4 variables including the user position and the receiver clock offset, therefore, at least 4 satellite information are needed to solve the problem.
However, the range measured by the receiver is affected by various error sources in the real world measurement. It is called the pseudorange. The pseudorange observation equation is

$$p = L_{\mathrm{d}} + \mathrm{c}(dt_r - dt_s) + e_{\mathrm{tr}} + e_{\mathrm{io}} + e, \tag{2.3}$$

where L_d is the geometric range between the satellite and the receiver, c is the speed of light, dt_r and dt_s donate the receiver clock offset and satellite clock offset, respectively. e_tr refers to the tropospheric error and e_io is the ionospheric error. e is the observation error including the multipath error and measurement error. These error sources will be explained in detail in Section 2.2.

2.2 GNSS error

Because the GNSS signal possesses relatively low power, it is easily to be affected by the sources of noise and errors during the transmission. As a result, the GNSS receiver measurement range will be contaminated. The GNSS signal error sources can be classified as clock offset error, signal propagation error, system error and intentional error [9]. The clock offset error and signal propagation error will be discussed in detail in the following.

2.2.1 Clock offset

Clock stability shows how well the clock oscillator frequency tolerates the fluctuations. Clock accuracy might be affected by factors such as the quality of the oscillator crystal and how the oscillator was assemble [10]. Satellites use atomic clock as their time system, which is tremendously accurate and normally fluctuates within 3 ns per second. The satellite clock error dt_s could be split in two terms:

$$dt_\mathrm{s} = dt_{\mathrm{s}_1} + dt_{\mathrm{s}_2}, \tag{2.4}$$

where dt_{s1} is the relativistic correction caused by the orbital eccentricity. And dt_{s2} could be calculated according to the navigation messages:

$$dt_{\mathrm{s}_2} = a_0 + a_1(t - t_0) + a_2(t - t_0)^2 \tag{2.5}$$

From the perspective of receiver clock, however, the manufacturers implement relatively cheaper clocks inside the vehicle, the time estimate stability is much lower for those in-car clocks comparing with satellite clocks. The quality of the receiver clock also differs from different manufacturers, resulting different clock offset. Therefore, in the present work, the clock offset is a reference value and can be different when implemented in the real world, and the influence of different clock error will also be illustrated in the result part. As time goes by, the bias between the satellites clock and receiver clock will grow up, which is clock offset. In terms of the range measurement error, the GNSS clock offset is about 2.59 m to 5.18 m per day [11].

2.2.2 Signal propagation error

The GNSS signal is electromagnetic wave, which can be easily influenced by the atmosphere disturbances during transmission, leading to ionospheric error and tropospheric error. Due to the signal reflections from surrounding buildings, the signal may reach the receiver through more than one path. This leads to the multipath error.

2.2.2.1 Ionospheric error

Ionosphere is the upper layer of the atmosphere and contains huge amount of free electrons. When the GNSS signal travels through the ionosphere, the ionosphere will influence the incidence angle due to the free electron space [12], as shown in Figure 2.1. The reflection or refraction phenomenon thereby will influence the measured distance from the perspective of GNSS receiver. Ionosphere is a disperse medium that makes the ionospheric error depending on frequency and the number of electrons. The expression for this error is

$$e_{\text{io}} = \frac{40.3 \times TEC}{f^2}, \tag{2.6}$$

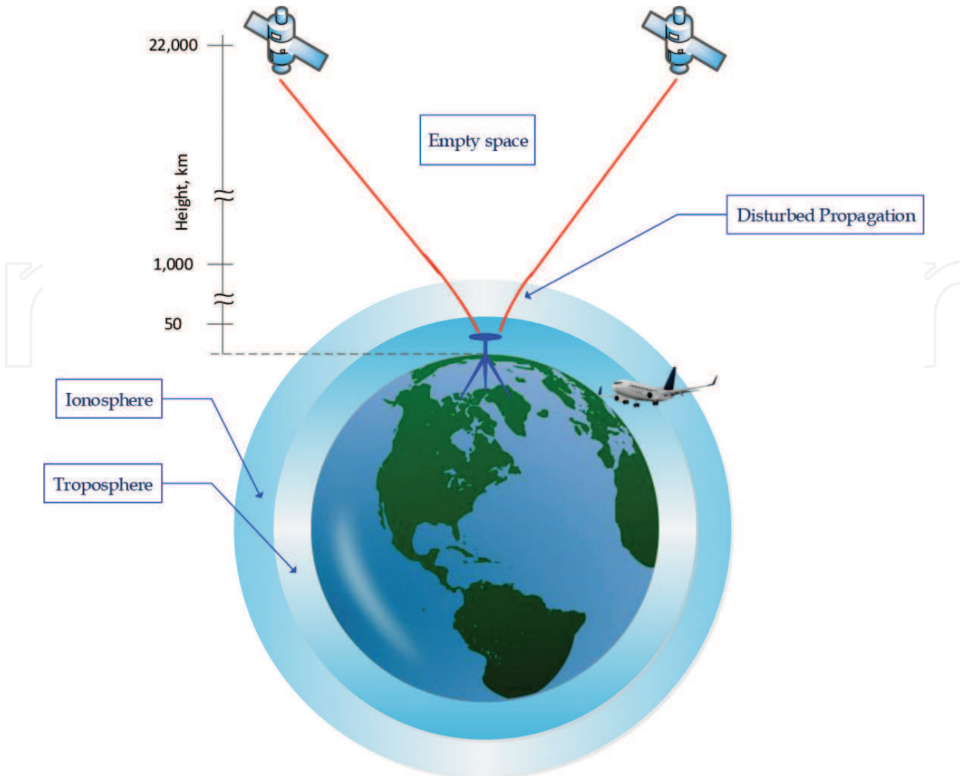

Figure 2.1: The ionospheric error and tropospheric error during signal transmission [13].

where the TEC is Total Electron Content, indicating the number of electrons in a tube of 1 m^2 cross section in the signal propagation direction and the f is the signal frequency in Hertz [9], which can be expressed by Eq(2.7)

$$TEC = \int n_e(s)ds, \tag{2.7}$$

where $n_e(s)$ is the location-dependent electron density, and s is the integration direction.

Normally, the ionospheric error can be up to 30 ns (100 m) in some cases[9].

2.2.2.2 Tropospheric error

Troposphere is the lowest layer of atmosphere and it composes dry gas and water vapor [14], making it a refraction layer which delays the GNSS signal as well, as shown in Figure 2.1. This kind of error contains two parts, the wet and dry, counting for 10% and 90% respectively. On the other hand, unlike the ionospheric error, the tropospheric error is frequency independent, meaning that it cannot be eliminated by measuring the link 1 (L1) frequency level (1575.42 MHZ) and link 2 (L2) frequency level (1227.60 MHz) signals from GPS. The tropospheric error is about from 2.5 m to 25 m depending on the elevation angle of the receiver [15].
One typical model for tropospheric error is from Collins [8]. The tropospheric error e_{tr} consists of the wet and dry components. The vertical delay t_{wet} and t_{dry} are computed from the receiver's height and estimates of five parameters,

$$t_{\text{dry}} = \left[1 - \frac{T_{\text{rate}} H_{\text{r}}}{T}\right]^{\frac{g}{R_{\text{d}} T_{\text{rate}}}} \cdot T_{0,\text{dry}}, \tag{2.8}$$

$$t_{\text{wet}} = \left[1 - \frac{T_{\text{rate}} H_{\text{r}}}{T}\right]^{\frac{g(\beta+1)}{R_{\text{d}} T_{\text{rate}}}-1} \cdot T_{0,\text{wet}}, \tag{2.9}$$

where, the parameters are summarized in the Table 2.1.

Table 2.1: The parameters for the tropospheric model

T_{rate}	Temperature "lapse" rate
β	Water vapour "lapse" rate
H_{r}	Receiver altitude
T	Temperature
R_{d}	Gas constant $287.054 J/Kg/K$
g	Gravity constant 9.80665 m/s^2
$T_{0,\text{dry}}$	Zero-altitude vertical delay terms (dry)
$T_{0,\text{wet}}$	Zero-altitude vertical delay terms (wet)

The tropospheric delay is calculated from the vertical delay according to the obliquity factor $M(\theta_{\text{e}})$

$$M(\theta_{\text{e}}) = \frac{1.001}{\sqrt{0.002001 + \sin^2(\theta_{\text{e}})}}, \tag{2.10}$$

where θ_{e} is the elevation angle. The tropospheric error is calculated as

$$e_{\text{tr}} = (t_{\text{dry}} + t_{\text{wet}}) \cdot M(\theta_{\text{e}}). \tag{2.11}$$

2.2.2.3 Multipath error

In the ideal situation, the GNSS signal could reach the GNSS receiver directly, which is called "line-of-sight" (LOS), as shown in Figure 2.2a and b. When there are buildings blocking the sight, the receiver could only track the reflected signal. In that case, signals are called as "non-line-of-sight" (NLOS) signals, as shown in Figure 2.2c.

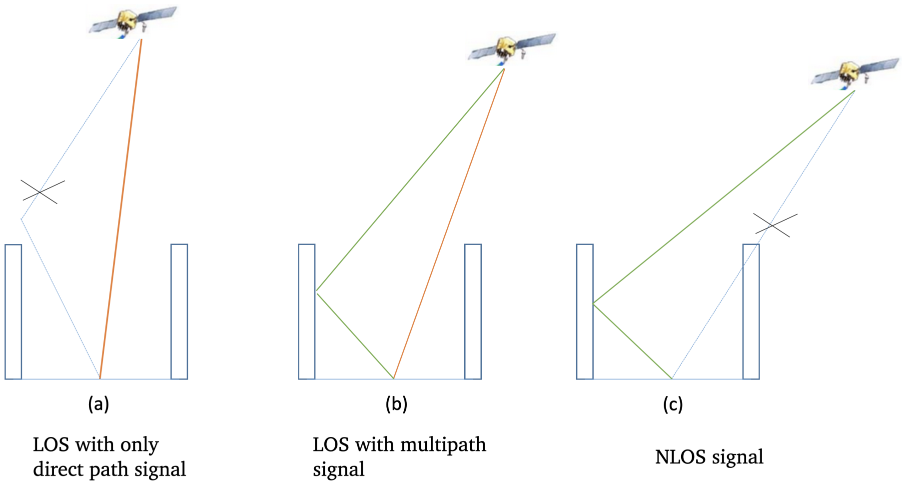

Figure 2.2: The satellite states: (a) LOS with only direct path signal (b) LOS with multipath signal (c) NLOS signal.

For the LOS situation, sometimes, the receiver will receive direct signal as well as other signals due to the reflection from the surroundings. When the direct signal merges with the reflected signal, there will be multipath error, as shown in Figure 2.2b. The reflected signal will always travel more distance than the direct signal. When the extra distance is larger than a certain range, which is $300m$, the receiver could detect that there exists the multipath. Because $300m$ is the time resolution for the GPS L1 signal that has a bandwidth of 1.023MHZ. In other words, there is a new chip about every 300 meters of distance. However, when the extra distance is less than 300 m, the received components blur together due to a lack of time resolution. In that case, the receiver views one blurry peak which is biased away from the direct path in the direction of the multipath, resulting in range measurement error. Because of the nature of signal transmission, the multipath signal is inevitable as long as there are buildings or other obstacles around the receiver, especially in the highly constrained environment [16].
For the NLOS situation in Figure 2.2c, since the receiver could only track the reflected signal, there will be a much larger multipath error. This could be the more severe multipath situation.

2.3 Stochastic channel model

In terms of statistic, a stochastic model is often established based on the historical data gathered from the experiment in the real world, by allowing one or certain variant inputs [17].
In the case of GNSS error simulation, the stochastic channel modeling is a useful method for establishing the error models, especially the multipath error. For example, with the collected Intermediate Frequency (IF) data, the multipath error can be extracted from the original data by certain algorithms [5]. After obtaining the multipath error data, one can characterize the probability distribution of this

error regarding to a variance input, for instance, the GNSS receiver elevation angle. The obtained stochastic model can be used for GNSS signal error modeling. For example, according to the error probability distribution above, any engineer could use this model to estimate the GNSS error regarding to a elevation angle.

2.4 Ray tracing model

Ray tracing proves to be an appropriate method for modeling the propagation of the electromagnetic waves, which is adopted for satellite-to-earth channel modeling [3]. In GNSS area, ray tracing is used to estimate the GNSS multipath signals given the satellite–reflector–antenna geometries. This method has a great potential in highly constrained multipath environments, such as urban scenarios.
The relevant research has been conducted to model the GNSS multipath error using ray tracing. Lawrence et al. [3] aim to use ray tracing to reconstruct the carrier-phase multipath error and remove it. They give a comprehensive description on the signal transmission, signal power loss, reflection process and antenna characteristic for the ray tracing model. Also, David et al. [4] use the ray tracing method to mitigate the pseudorange multipath error. Originally, they propose the urban trench model [4] to identify the section of the street and classify the satellites as visible and invisible type. For the correction of the multipath error, the number of reflection is considered [4]. Moreover, Shiwen et al. [6] use the ray tracing to develop the detection algorithms for satellite exclusion and compare different satellite exclusion algorithms.
In this chapter, the GNSS error sources are summarized and the multipath error is explained in detail. Two methods for the GNSS error including the stochastic model and ray tracing model are introduced. Based on the theories above, we will present the methods we use to model the GNSS error in the next chapter.

3
Methods

This part will introduce the general properties of this ray tracing model, including the assumptions and functions. The earth geometry and the satellite track model will be introduced. The signal reflection and power attenuation when transmitting will be explained, as well as the software and algorithm during the development.

3.1 Satellite generation

The satellite model used in the present ray tracing model is generated by the Satellite Communications Toolbox in the MATLAB R2022b. There are 31 satellite models in total, each one of them is built based on the real satellite ephemeris data collected on the 30th of May, by CelesTrack, which is a non-profit organization focusing on making data and other resources freely available to the space community. Those ephemeris data can be download directly from the website (https://celestrak.com/). The generated satellite model is shown in Figure 3.1a, with the earth located in the center. The red points and circle (or ellipse) represent the different satellites and track, surrounding the earth.

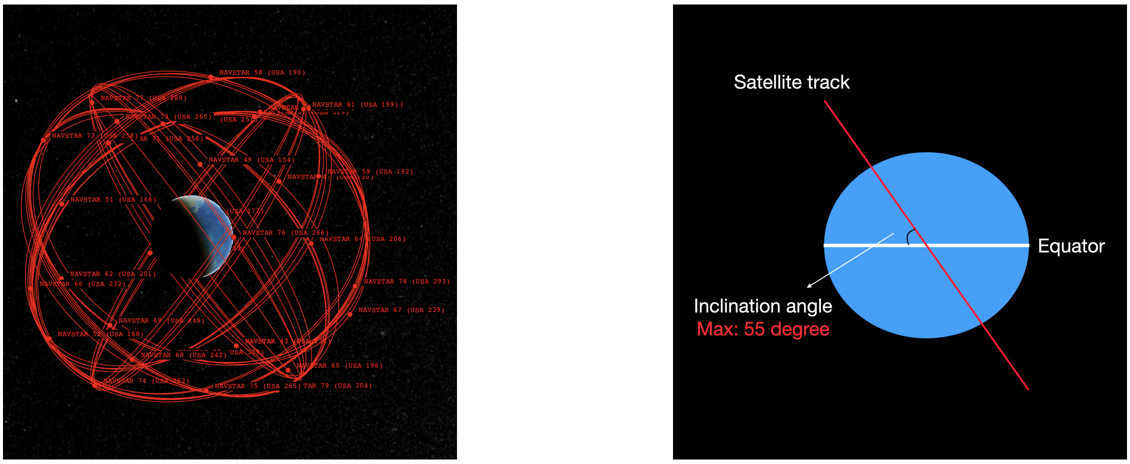

(a) **(b)**

Figure 3.1: Satellite model: (a) Satellite distribution (b) Satellite track inclination.

As one can imagine, when projecting the model into a 2D plane, there will be an inclination between the satellite track and the equator, see Figure 3.1b. For

GPS system, the maximum satellite track inclination angle is 55 degrees, which means locations with latitudes from 55 to 90 degrees North and South will have the limitation for satellite geometry in sight, e.g., impossible to have 90 degree-elevation angle.
From the Satellite Communication toolbox, all the satellites are settled in the Earth-Centered-Earth-Fixed (ECEF) coordinate system, with the earth center as the origin, Z_{ECEF} axis points to the north pole, X_{ECEF} axis points to the intersection of equator and 0 degree longitude, then the Y_{ECEF} axis is settled following the right-hand system. To simplify the street scenario creation work in the later stage, it is better to use the East-North-Up (ENU) coordinate system, which uses the location of satellite receiver as the origin. Note that in the present work, the capital X, Y and Z are used to represent the coordinates in ECEF system, their lower case x, y and z are used for the ENU system.
From the Figure 3.2, the transformation from ECEF to ENU can be done in the following steps: translate from the earth center to the receiver location, rotate around the Z_{ECEF} axis by $90 + \lambda$ degree, then rotate around the X_{ECEF} axis by $90 - \phi$ degree, after which the coordinates in ECEF system X, Y and Z will become x, y and z coordinates in the ENU system, respectively. In the description above, λ and ϕ represent the longitude and latitude of the receiver location, respectively. Note that the positive values are used for the north latitude and east longitude, the negative values are for the south latitude and west longitude, and all the satellites will be transformed from ECEF to ENU coordinate system in the present ray tracing model.

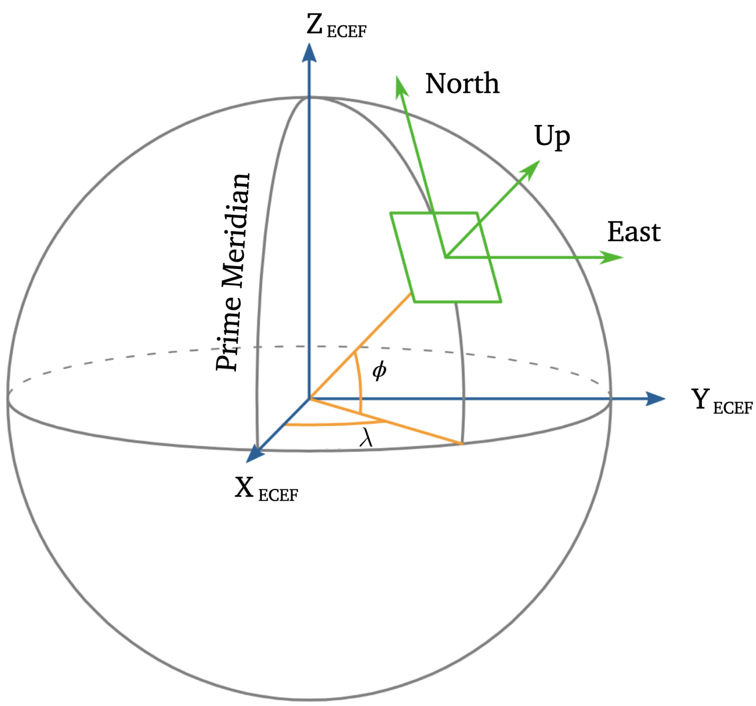

Figure 3.2: ECEF and ENU coordinate system.

In mathematical model, the 3D coordinate transformation will use one translation matrix and two rotation matrices. In homogeneous coordinates, the translation matrix is

$$T = \begin{bmatrix} 1 & 0 & 0 & -\mathrm{X_r} \\ 0 & 1 & 0 & -\mathrm{Y_r} \\ 0 & 0 & 1 & -\mathrm{Z_r} \\ 0 & 0 & 0 & 1 \end{bmatrix}, \tag{3.1}$$

where the $\mathrm{X_r}$, $\mathrm{Y_r}$ and $\mathrm{Z_r}$ are the coordinates of the receiver in ECEF system. The two rotation matrices are

$$\mathrm{Yaw}: R_z = \begin{bmatrix} \cos(\theta_\mathrm{y}) & -\sin(\theta_\mathrm{y}) & 0 & 0 \\ \sin(\theta_\mathrm{y}) & \cos(\theta_\mathrm{y}) & 0 & 0 \\ 0 & 0 & 1 & 0 \\ 0 & 0 & 0 & 1 \end{bmatrix}^T \tag{3.2}$$

$$\mathrm{Roll}: R_x = \begin{bmatrix} 1 & 0 & 0 & 0 \\ \cos(\theta_\mathrm{r}) & -\sin(\theta_\mathrm{r}) & 0 & 0 \\ \sin(\theta_\mathrm{r}) & \cos(\theta_\mathrm{r}) & 0 & 0 \\ 0 & 0 & 0 & 1 \end{bmatrix}^T, \tag{3.3}$$

where the yaw angle θ_y is $90 + \lambda$ and roll angle θ_r is $90 - \phi$. The reason why using transpose here is that the transformation is from ECEF to ENU, the yaw or roll rotation direction is contrary to the right-hand law. Due to the nature of rotation matrices, e.g., orthogonal matrices, the rotation inverse matrices can be expressed as their transpose. As the result, if the satellite coordinate is known as $(\mathrm{X_s}, \mathrm{Y_s}, \mathrm{Z_s})$ in the ECEF system, then the satellite can be transformed into the ENU system

$$\begin{pmatrix} \mathrm{x_s} \\ \mathrm{y_s} \\ \mathrm{z_s} \end{pmatrix} = R_\mathrm{x} \cdot R_\mathrm{z} \cdot T \cdot \begin{pmatrix} \mathrm{X_s} \\ \mathrm{Y_s} \\ \mathrm{Z_s} \end{pmatrix}. \tag{3.4}$$

3.2 Scenario generation

For the scenario generation, we consider the urban trench model [4]. In our model, the section of the street is assumed as a trench, defined by several parameters ($W =$ street width, $H =$ street height range, $P =$ street width ratio). For the simplification, each building is referred as a 3D plane and the receiver is simplified as a point with the given lateral distance to the left building, the lateral distance is the product of W and P.

In our model, the street could be created by the given street direction, start point, width and length. This means we could define the position and direction of the street and combine them to generate the urban scenario. The height and width of each building in the street can also be defined. One generated scenario is presented in Figure 3.3.

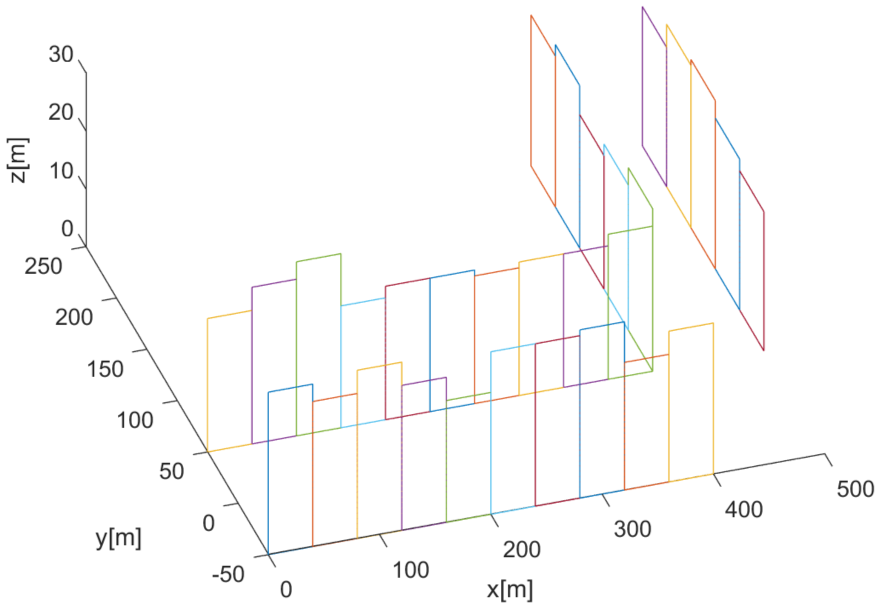

Figure 3.3: One example for the visualization of a generated urban scenario from MATLAB.

3.3 Signal transmission

This section presents the simulation of the GNSS signals in the urban environment. First, three different satellite states are explained. The satellite-receiver-geometry is adopted to define the potential signal type. More important, this section describes how to check whether there is direct signal or reflected signal for each satellite. Also, the property of signal such as the power is calculated. According to the signal type and power, the satellites could be classified into three states and the multipath error could be computed for each satellite.

3.3.1 The satellite states

At one time, one receiver may receive more than one signal from one satellite. For one satellite, there could be three situations: LOS with only direct path signal, LOS with multipath signal and NLOS, as shown in Figure 2.2. If there exists the direct path signal and no reflection in the street, we conclude there is LOS with only direct path signal (Figure 2.2a). If there are direct signal as well as reflected signal, it will be the LOS with multipath signal (Figure 2.2b). If the direct path signal is blocked and the receiver only receives the reflected signal, this situation is called as NLOS (Figure 2.2c).

3.3.2 The direct/reflected signal determination

According to the relative position between the satellite, receiver and buildings, the satellite signals can be classified as direct and reflected signals. During the process of programming, however, deciding whether it is direct or reflected signal is not that obvious.

At first, the satellite-receiver-geometry is determined. Considering the relative position between the satellite and the street, the satellite could be on the left, right side or just in the middle (within the street width) of the street. According to the street direction, street start point and satellite position, we could define which side the satellite is for the street. If the street is along the x axis, then the y coordinates for both the satellite and the street will be used to get the satellite-receiver-geometry. If the street is along the y axis, the comparison will happen to x coordinates. Moreover, if the street direction is random, we will judge the relative position of the satellite and street through the x and y coordinates.

Due to the satellite-receiver-geometry, we could define the possible signal type for each buildings of the street, which is presented in Algorithm 1. If the satellite is on the left side of the street, there might be the reflected signal from the right building and the direct path signal could only be blocked by the left building, vise versa. If the satellite is in the middle of the street, which is rarely to happen, there will be direct path signal and possibly the reflected signal coming from buildings in both sides of the street.

Algorithm 1 The potential signal type due to the satellite-receiver-geometry

if satellite is on the left **then**
    Determine if the left building blocks the direct signal
    Determine if there is reflected signal from the right building
else if satellite is on the right **then**
    Determine if the right building blocks the direct signal
    Determine if there is reflected signal from the left building
else
    There exists the direct signal
    Determine if there is reflected signal from the left building
    Determine if there is reflected signal from the right building
end if

Since the street is composed of lots of buildings with different heights, we firstly consider the scenario of one building. In order to define whether there is direct path signal, we use the geometrical method to determine if the signal ray intersects with the scenario while propagation. More specifically, for a 3D line and plane, they can only intersect at one point if they are not parallel to each other. In this case, we use one building point and the normal vector to determine a building plane, see Eq.(3.5), where $(\mathrm{A}, \mathrm{B}, \mathrm{C})$ is the normal vector of the plane and (x_0, y_0, z_0) is an arbitrary point on the plane.

$$\mathrm{A}(x - x_0) + \mathrm{B}(y - y_0) + \mathrm{C}(z - z_0) = 0 \tag{3.5}$$

Then using the satellite point (x_s, y_s, z_s) and receiver point (x_r, y_r, z_r) to create a 3D line

$$\frac{y - y_s}{y_s - y_r} = \frac{x - x_s}{x_s - x_r}. \tag{3.6}$$

By combining Eq.(3.5) and Eq.(3.6), the intersection point can be determined. With 4 corners of the building as the limitation, one can decide if the intersection point is on the plane or not. Hence, if the intersection point is not on the building surface, there is a direct path signal.

On the other hand, if we want to determine whether there is reflected signal from this building, the symmetrical point of the receiver need to be found first,as shown in Figure 3.4b, then decide if there is direct path, which is 'phantom' signal between the satellite and the symmetrical point, in the same way of determining the direct path signal. We call it 'phantom' signal because it doesn't exist. If the 'phantom' signal is blocked by the plane, there will be reflected signal from the building. The illustration of the two cases for one building is presented in Figure 3.4. Note that for the one building case, if there is no direct path signal, then there will be no signal received by the receiver.

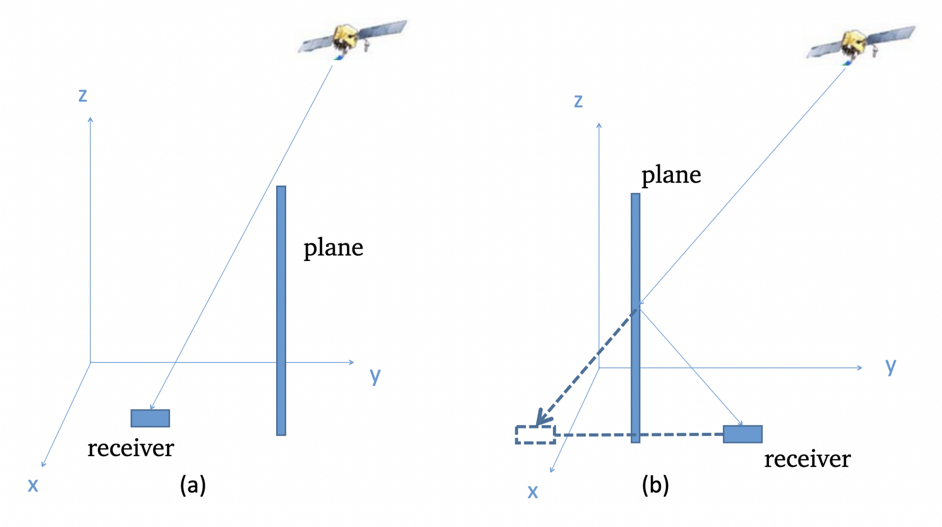

Figure 3.4: The LOS geometric determination for the scenario of one building (a) Direct path signal (b) Reflected signal.

Considering the whole street, the direct/reflected signal determination is related to every building. For the direct signal case, only if there exists the direct path signal for all the buildings in this street, we conclude there is the direct signal for the street. On the contrary, for the reflected signal, if there exists the reflected signal for one building, we conclude there is the reflected signal for the street. To illustrate more clearly, we assume the satellite is on the left side of the street and there are 10 buildings both in the left and right side of the street, Algorithm 2 is the direct/reflected signal determination for streets. The state of the *direct* and *reflect* in Algorithm 2 represents whether there is the direct/reflect signal in the street.

Algorithm 2 The direct/reflected signal determination for streets

Input: The coordinates of receiver and street
Output: $direct$, $reflect$

$direct$ = TRUE
$reflect$ = FALSE
$n = 10$
$i = 1$
while $i < n$ **do**
    Determine if the i_{th} building on the left street has the direct signal
    if the i_{th} building does not have direct signal **then**
        $direct$ = FALSE
    end if
    Determine if there is reflected signal from the i_{th} building on the right street
    if the i_{th} building has reflected signal **then**
        $reflect$ = TRUE
    end if
    $i \leftarrow i + 1$
end while

3.3.3 Signal property

The GNSS signal properties consist of the power and the polarization of the signal. Generally, the signals transmitted by the satellites are right-hand circularly polarized (RCP). After reflection, the signals are always left-hand circularly polarized (LCP) [16]. For some expensive and physically large antennas, the polarization state of signals will influence the received power. However, vehicle antennas have a poor axial ratio, which means the signals with RCP and LCP are received with the similar power. Therefore, the polarization of the GNSS signal does not have great influence on the signal reception for vehicle. Therefore, we mainly consider the power of the signal, which will influence the weight of each signal in the multipath error calculation.

The power loss in the GNSS transmission mainly includes the power loss in the obstacle-free path and the reflection process. For the signals transmitted in the obstacle-free path, the free space equation derived from the Friis transmission formula [18] is used to calculate the signal power loss

$$\rho_{\mathrm{f}} = (\frac{4\pi df}{\mathrm{c}})^2, \tag{3.7}$$

where d represents the distance between the satellite and the antenna, f is the signal frequency, and c is the speed of light.

The power loss due to reflection depends on the relative permittivity and the Fresnel reflection coefficient ρ_r. The perpendicular Fresnel reflection coefficient [19] is

$$\rho_{\perp} = \frac{\cos\theta_i - \sqrt{\epsilon_2/\epsilon_1 - \sin^2\theta_i}}{\cos\theta_i + \sqrt{\epsilon_2/\epsilon_1 - \sin^2\theta_i}}, \tag{3.8}$$

where θ_i stands for angle of incidence, ϵ_1 and ϵ_2 represent the permitivity of the first material (air) and second material (brick).
The parallel Fresnel reflection coefficient is

$$\rho_{\parallel} = \frac{-(\epsilon_2/\epsilon_1)\cos\theta_i + \sqrt{\epsilon_2/\epsilon_1 - \sin^2\theta_i}}{(\epsilon_2/\epsilon_1)\cos\theta_i + \sqrt{\epsilon_2/\epsilon_1 - \sin^2\theta_i}}. \tag{3.9}$$

The total reflection coefficient is

$$\rho_{\mathrm{r}} = \rho_{\parallel}\cos^2\theta_i + \rho_{\perp}\sin^2\theta_i. \tag{3.10}$$

Considering the free space path loss and the reflection loss, the signal power at the receiver is

$$PL = P_0 \cdot \rho_{\mathrm{r}} \cdot \rho_f, \tag{3.11}$$

where P_0 denotes the signal power at the satellite. For the power loss of the direct signal, the reflection coefficient ρ_{r} is assumed as unit 1.

3.3.4 Multipath error computation

For each satellite, the receiver calculates the total path length L_{c} by linearly combining the path length of direct and reflected signal due to the power

$$L_{\mathrm{c}} = \frac{L_{\mathrm{d}}P_{\mathrm{d}} + L_{\mathrm{m}}P_{\mathrm{m}}}{P_{\mathrm{d}} + P_{\mathrm{m}}}, \tag{3.12}$$

where the P_{d} and P_{m} are the powers of the direct signal and reflected signal. And L_{d} and L_{m} are the path length of the direct signal and reflected signal. If the direct signal or reflected signal is non-existed, we put the P_{d} or P_{m} as zero.
After computing the total path length for each situation, the differential path delay compared to the true path length is calculated, which we call it 'multipath error' in this paper. And we use the direct path length as the true path length between the satellite and receiver. For example, for the LOS with only direct path signal situation, the multipath error is assumed to be zero. The multipath error is

$$e_{\mathrm{m}} = L_{\mathrm{c}} - L_{\mathrm{d}}. \tag{3.13}$$

3.4 GNSS error modeling

Besides the multipath error, the ionospheric error, tropospheric error, clock offset error and receiver noise error are considered for the calculation of the pseudorange in the ray tracing model.

3.4.1 Ionospheric error and tropospheric error

The GPS Klobuchar model [7] is used to model the ionospheric error (e_{io}). Given the geomagnetic location and local time t_0, the mean vertical ionospheric time delay (t_{io}) at L1 is defined as

$$t_{\mathrm{io}} = A_1 + A_2 \cos\left[\frac{2\pi(t_0 - A_3)}{A_4}\right], \tag{3.14}$$

where A_1 represents the constant night-time value, A_2 means the amplitude, A_3 is a phase shift at 14.00 time and A_4 represents the period of the cosine function.
The vertical path delay $e_{\mathrm{io}}^{\perp}$ is

$$e_{\mathrm{io}}^{\perp} = \mathrm{c} \cdot t_{\mathrm{io}}. \tag{3.15}$$

In order to convert the vertical path delay to the ionospheric delay, the obliquity factor $M(\theta_{\mathrm{e}})$ is computed according to the elevation angle θ_{e}

$$M(\theta_{\mathrm{e}}) = 1 + 16(0.53 - \theta_{\mathrm{e}})^3. \tag{3.16}$$

The ionospheric error is

$$e_{\mathrm{io}} = e_{\mathrm{io}}^{\perp} \cdot M(\theta_{\mathrm{e}}). \tag{3.17}$$

For the tropospheric error, we choose the model from Collins [8], which is explained in Chapter 2.

3.4.2 Measurement error and clock offset error

As described in [20], the measurement error standard deviation from mass market manufacture is around 0.49. Therefore, the measurement error is modeled by a number with normal randomization using 0.49 as the standard deviation. The clock error is at the nanosecond [9].

3.5 Least square method for localization

3.5.1 Linearization

To estimate the approximate position of the GNSS receiver, one of the methods is least squared (LS) method. In the ENU (or ECEF) coordinate system, the position of the receiver can be represented by three component $\mathrm{x_r}$, $\mathrm{y_r}$ and $\mathrm{z_r}$. While there is clock offset between the satellite and receiver, which is also unknown. Thus, 4 unknowns need to be solved for the position estimation, 4 equations need to be established at least. For each satellite in sight, there is one observation equation of the pseudorange. Therefore, 4 satellites in sight will be enough to solve the localization problem. The expression of the observation equation for one satellite is expressed in Eq.(2.3).
From the description above, the geometric range can be computed as

$$L_{\mathrm{d}} = \sqrt{(x_s - x)^2 + (y_s - y)^2 + (z_s - z)^2}, \tag{3.18}$$

where (x, y, z) is the coordinate for the receiver and the (x_s, y_s, z_s) is the coordinate for one satellite. From the Eq.(3.18), however, the geometric observation range is nonlinear, the linearization is necessary before using the LS. Regard the geometric range L_{d} as a function of (x, y, z), e.g., $f(x, y, z)$, and start from the center of earth (the origin $(0, 0, 0)$), the estimation of the receiver position can be improved by iteration. For each iteration, the position can be improved by Δx_{i}, Δy_{i}, and Δz_{i}. Hence, after one iteration, the receiver position updates like

$$\begin{aligned} x_{\mathrm{i+1}} &= x_{\mathrm{i}} + \Delta x_{\mathrm{i}} \\ y_{\mathrm{i+1}} &= y_{\mathrm{i}} + \Delta y_{\mathrm{i}} \\ z_{\mathrm{i+1}} &= z_{\mathrm{i}} + \Delta z_{\mathrm{i}}. \end{aligned} \tag{3.19}$$

Using the Taylor Expansion to get the first order of $f(x_{\mathrm{i}} + \Delta x_{\mathrm{i}}, y_{\mathrm{i}} + \Delta y_{\mathrm{i}}, z_{\mathrm{i}} + \Delta z_{\mathrm{i}})$

$$\begin{aligned} f(x_{\mathrm{i+1}}, y_{\mathrm{i+1}}, z_{\mathrm{i+1}}) = f(x_{\mathrm{i}}, y_{\mathrm{i}}, z_{\mathrm{i}}) \\ + \frac{\partial f(x_{\mathrm{i}}, y_{\mathrm{i}}, z_{\mathrm{i}})}{\partial x_{\mathrm{i}}} \Delta x_{\mathrm{i}} \\ + \frac{\partial f(x_{\mathrm{i}}, y_{\mathrm{i}}, z_{\mathrm{i}})}{\partial y_{\mathrm{i}}} \Delta y_{\mathrm{i}} \\ + \frac{\partial f(x_{\mathrm{i}}, y_{\mathrm{i}}, z_{\mathrm{i}})}{\partial z_{\mathrm{i}}} \Delta z_{\mathrm{i}}, \end{aligned} \tag{3.20}$$

where the partial deviation terms are

$$\begin{aligned} \frac{\partial f(x_{\mathrm{i}}, y_{\mathrm{i}}, z_{\mathrm{i}})}{\partial x_{\mathrm{i}}} &= -\frac{x_s - x_{\mathrm{i}}}{L_{\mathrm{d}}} \\ \frac{\partial f(x_{\mathrm{i}}, y_{\mathrm{i}}, z_{\mathrm{i}})}{\partial y_{\mathrm{i}}} &= -\frac{y_s - y_{\mathrm{i}}}{L_{\mathrm{d}}} \\ \frac{\partial f(x_{\mathrm{i}}, y_{\mathrm{i}}, z_{\mathrm{i}})}{\partial z_{\mathrm{i}}} &= -\frac{z_s - z_{\mathrm{i}}}{L_{\mathrm{d}}}. \end{aligned} \tag{3.21}$$

If we iterate the Eq.(3.19), (3.20), (3.21) and (3.18) back to the Eq.(2.3), for each iteration i and satellite, the linearized observation equation is

$$\begin{aligned} p_{\mathrm{i}} =& L_{\mathrm{d}} - \frac{x_s - x_{\mathrm{i}}}{L_{\mathrm{d}}} \Delta x_{\mathrm{i}} - \frac{y_s - y_{\mathrm{i}}}{L_{\mathrm{d}}} \Delta y_{\mathrm{i}} - \frac{z_s - z_{\mathrm{i}}}{L_{\mathrm{d}}} \Delta z_{\mathrm{i}} \\ &+ \mathrm{c}(dt_{\mathrm{r,i}} - dt_s) + e_{\mathrm{tr,i}} + e_{\mathrm{io,i}} + e_i. \end{aligned} \tag{3.22}$$

3.5.2 Applying LS

As mentioned before, the estimated position will be calculated by iterations. For each iteration, we use the least square method to get the position components which are used to upgrade the current position estimation. This LS problem can be formed as

$$\min ||\vec{\boldsymbol{A}}\vec{\boldsymbol{x}} - \vec{\boldsymbol{b}}||_2. \tag{3.23}$$

From which we need to find a proper $\vec{\boldsymbol{x}}$ giving formula 3.28 the minimum value. To achieve this, the Eq.(3.22) need to be reorganized as

$$\begin{bmatrix} -\frac{x_{\mathrm{s}} - x_{\mathrm{i}}}{L_{\mathrm{d}}} & -\frac{y_{\mathrm{s}} - y_{\mathrm{i}}}{L_{\mathrm{d}}} & -\frac{z_{\mathrm{s}} - z_{\mathrm{i}}}{L_{\mathrm{d}}} \end{bmatrix} \begin{bmatrix} \Delta x_{\mathrm{i}} \\ \Delta y_{\mathrm{i}} \\ \Delta z_{\mathrm{i}} \end{bmatrix} = p_{\mathrm{i}} - L_{\mathrm{d}} + c dt_s - e_{\mathrm{tr,i}} - e_{\mathrm{io,i}} - e_{\mathrm{i}}. \tag{3.24}$$

This linear equation is for a single satellite. If there are m ($m >= 4$) satellites available, there will be a system of linear equations with unique solution

$$\vec{\boldsymbol{A}} = \begin{bmatrix} -\frac{x_{\mathrm{s},1}-x_{\mathrm{i}}}{L_{\mathrm{d},1}} & -\frac{y_{\mathrm{s},1}-y_{\mathrm{i}}}{L_{\mathrm{d},1}} & -\frac{z_{\mathrm{s},1}-z_{\mathrm{i}}}{L_{\mathrm{d},1}} & 1 \\ -\frac{x_{\mathrm{s},2}-x_{\mathrm{i}}}{L_{\mathrm{d},2}} & -\frac{y_{\mathrm{s},2}-y_{\mathrm{i}}}{L_{\mathrm{d},2}} & -\frac{z_{\mathrm{s},2}-z_{\mathrm{i}}}{L_{\mathrm{d},2}} & 1 \\ -\frac{x_{\mathrm{s},3}-x_{\mathrm{i}}}{L_{\mathrm{d},3}} & -\frac{y_{\mathrm{s},3}-y_{\mathrm{i}}}{L_{\mathrm{d},3}} & -\frac{z_{\mathrm{s},3}-z_{\mathrm{i}}}{L_{\mathrm{d},3}} & 1 \\ \vdots & \vdots & \vdots & \vdots \\ -\frac{x_{\mathrm{s,m}}-x_{\mathrm{i}}}{L_{\mathrm{d,m}}} & -\frac{y_{\mathrm{s,m}}-y_{\mathrm{i}}}{L_{\mathrm{d,m}}} & -\frac{z_{\mathrm{s,m}}-z_{\mathrm{i}}}{L_{\mathrm{d,m}}} & 1 \end{bmatrix} \tag{3.25}$$

$$\vec{\boldsymbol{x}} = \begin{bmatrix} \Delta x_{\mathrm{i}} & \Delta y_{\mathrm{i}} & \Delta z_{\mathrm{i}} & cdt_{\mathrm{r,i}} \end{bmatrix}^{\mathrm{T}} \tag{3.26}$$

$$\vec{\boldsymbol{b}} = \begin{bmatrix} b_{\mathrm{i},1} & b_{\mathrm{i},2} & b_{\mathrm{i},3} & \cdots & b_{\mathrm{i,m}} \end{bmatrix}^{\mathrm{T}}, \tag{3.27}$$

where $\boldsymbol{b}_{\mathrm{i}}$ is $p_{\mathrm{i}} - L_{\mathrm{d}} + cdt_{\mathrm{i}} - e_{\mathrm{tr,i}} - e_{\mathrm{io,i}} - e_{\mathrm{i}}$. The position components of solution $\vec{\boldsymbol{x}}_{\mathrm{i}}$ needs to be combined with the current receiver position $\begin{bmatrix} x_{\mathrm{i}} & y_{\mathrm{i}} & z_{\mathrm{i}} \end{bmatrix}^{\mathrm{T}}$ to get the position updating for the next iteration. The iteration continues until the terms Δx_{i}, Δy_{i}, and Δz_{i} are at the meter level.

3.6 The verification: Monte Carlo method

The statistic distribution of the multipath error using the ray tracing could be analysed using Monte Carlo method. Monte Carlo simulation replies on the repeated random sampling and statistical analysis to calculate the results [21], which is adopted in our model to analyze the GNSS multipath error.

In the Monte Carlo simulation, we identify the statistical distribution of the height of each building and the position of the receiver. The height of each building is randomly distributed within the given height range of the street. And the receiver is located randomly on the ground of the street. Then, samples are drawn for each distribution and put into the proposed ray tracing model. The outputs of the ray tracing model are mainly multipath error and position estimation error.

After large amount of simulation, the statistical analysis is performed on the outputs, mainly the empirical Cumulative Distribution Function (CDF) plot. For a value t in outputs, the empirical CDF F(t) is the proportion of the values in outputs less than or equal to t. The results will be discussed in detail in the following sections.

4

Results and Analysis

In this chapter, the simulation scenarios and parameters are presented first. Also, we explain the performance metrics for the proposed system, including the position error and multipath error. The simulation results for different cases are presented and analyzed.

4.1 Scenario and simulation parameters

In the simulation, the receiver is located at Gothenburg with the latitude of 57.7 degree. The baseline scenario is the street with the height of around 25m and width of 15m. The receiver is located randomly in the street. The effects of different factors on the multipath error are also explored, including the street width, lateral location of the receiver and elevation angle. To explore these factors we set different scenarios in the simulation. More specifically, the street widths are selected every 10m between 10m to 120m. The street width ratios are selected as 0.1, 0.2, 0.3, 0.4 and 0.5. The elevation angles are distributed randomly from 0 to 85 degree.

4.2 Performance metrics

The performance metrics for the proposed GNSS system are mainly the estimated position error and multipath error. For each epoch in the simulation, the estimated position error of the proposed model is calculated as

$$e_{\mathrm{x}} = |\hat{x} - x_{\mathrm{r}}| \tag{4.1}$$

$$e_{\mathrm{y}} = |\hat{y} - y_{\mathrm{r}}| \tag{4.2}$$

$$e_{\mathrm{z}} = |\hat{z} - z_{\mathrm{r}}| \tag{4.3}$$

The e_{x} represents the estimated position error in x direction, which is parallel to the street direction. The e_{y} represents the estimated position error in y direction, which is perpendicular to the street direction. The e_{z} means the estimated error on the z axis.
The multipath errors for each satellite are calculated at the level of pseudorange, which is the difference between the calculated path length and the true path length for each satellite, as explained in Section 3.4.4.

4.3 Results and discussion

4.3.1 Position error

First, we consider the position error distribution for the baseline scenario. After the simulation for 10000 times, the CDF plot of e_x, e_y, e_z is Figure 4.1. From the Figure 4.1 we could see the position errors along the street are the lowest among three directions. 90 percent of the e_x are less than 2m, which could allow the user to have fairly accurate location information in the street direction. However, most of the e_z are distributed within 20m. And the accuracy of the estimated position error perpendicular to the street is the lowest, which is e_y within 25m. The reason behind this may be that the reflected signal mainly reflects in the direction perpendicular to the street, which influences the e_y. This means the multipath effect has great influences on the localization in the direction perpendicular to the street.
In the simulation above, we assume the clock offset error is distributed between -500ms to 500 ms. If we assume the clock offset is within 10 ns and run the simulation, the position error is different as shown in Figure 4.2. It is clear that the position error on x direction has increased compared to the Figure 4.1. This means the selection of clock offset could largely affect the position error in the street direction.

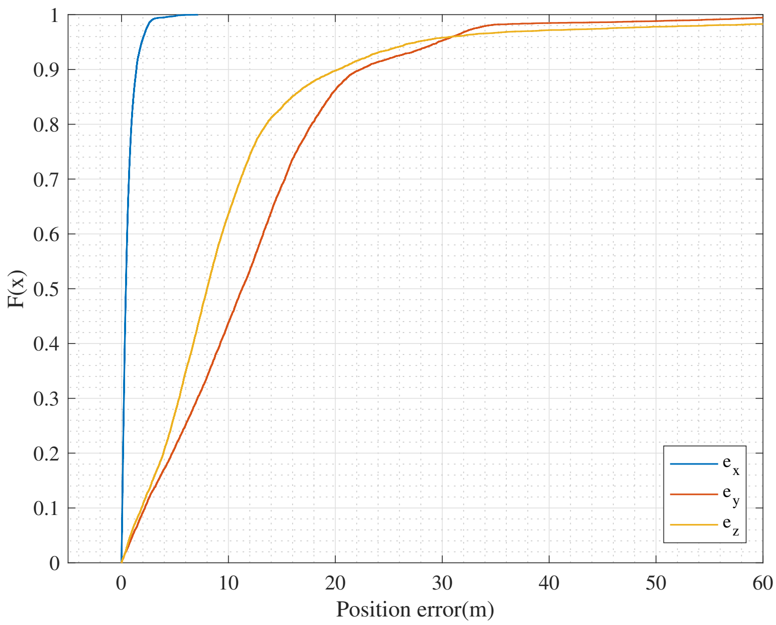

Figure 4.1: The CDF plot for position estimation errors in X, Y and Z direction with the clock offset between -500ms to 500ms.

4.3.2 Multipath error

The multipath errors for each satellite are calculated as Section 3.4.4. These errors are classified in Figure 4.3 according to the three satellite situations: only direct path signal, only reflected signal and multipath signal. Since we assume the multipath

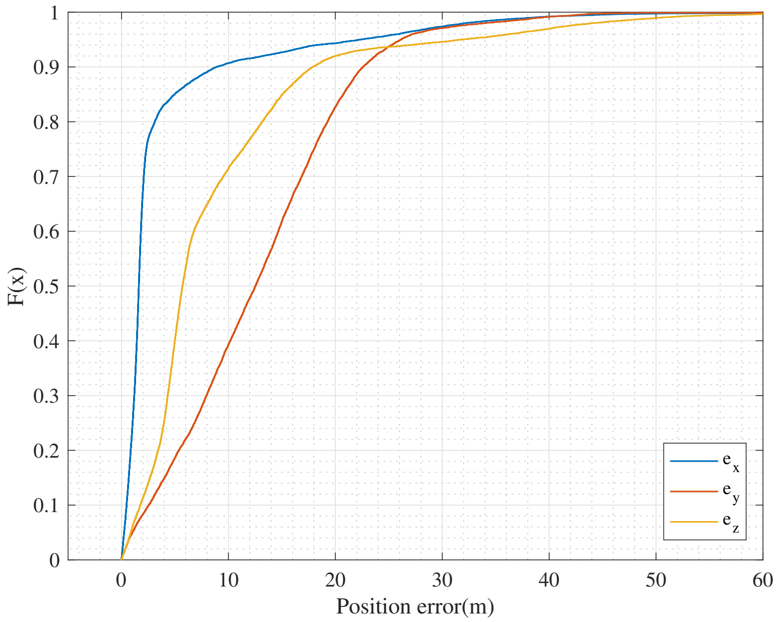

Figure 4.2: The CDF plot for position estimation errors in X, Y and Z direction with the clock offset within 10ns.

error for direct path signal is 0, we could see the multipath errors for this case are all zero. The multipath errors for multipath satellite are relatively low, within 2m, since there are both direct and reflected signals. While the errors for only reflected signal case reach to 25m, which are much larger than those of multipath satellite. This could illustrate the only reflection case could be the most severe situation for the localization.

In order to analyze the multipath error further, the effects of different factors on the multipath error are explored, including the street's width, the lateral position of the receiver and the satellite elevation angle. What is more, we want to figure out the reason why these factors influence the multipath error.

Considering the street's width, the relationship between the multipath errors and the width of the streets is shown in Figure 4.4. This figure is divided into two subplots since the errors have different trends in different width ranges.

On the left subplot in Figure 4.4, the multipath errors increase as the width of streets increases from 10m to 40m. The reason might be that the reflection path length has increased as the width of street increases. While, as the width of street continues increasing, the trend for the right subplot in Figure 4.4 is different from the left one. We only consider the majority of the error, which is the error lower than 25m. In this case the widest street has the lowest error. This is because that the reflection signals disappear when the street is wide enough.

Through the analysis, the reflected path length of the signal and the ratio of the reflected signal both contribute to the distribution of the multipath error. The reflected path length has larger effect on the multipath error when the street is within 50m. While the ratio of the reflected signal contributes more to the multipath error when the street width is within 50m to 120m.

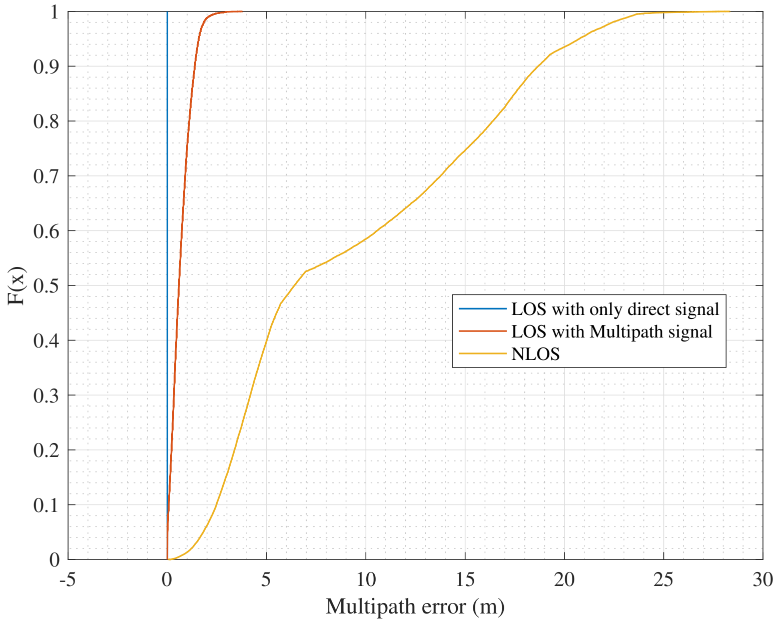

Figure 4.3: The CDF plot for multipath errors with different situations.

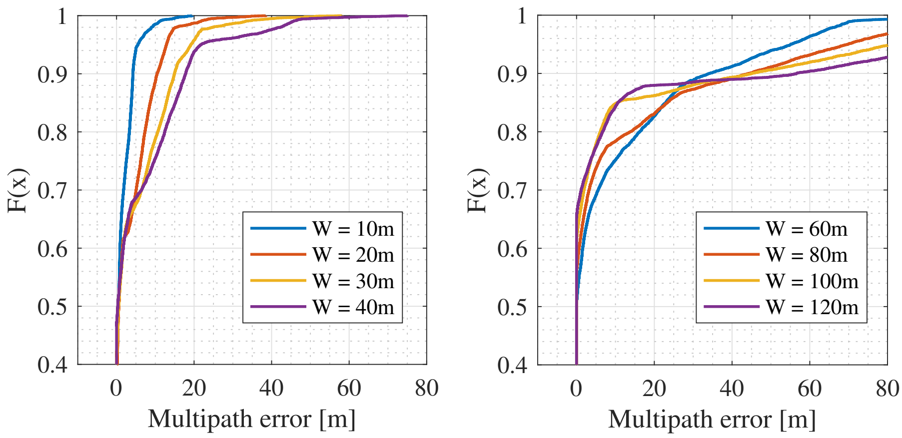

Figure 4.4: The CDF plot for multipath errors with different street widths.

Moreover, the lateral position of the receiver proves to closely related to the distribution of multipath error. For different street width ratios P, the multipath errors are distributed in Figure 4.5.
For the receiver located close to the wall, which means P is between 0 to 0.1, the multipath errors are clustered in three ranges: 0-2 m, 6-7 m and 16-17 m. The reflected signal from the near building could lead to the error within 2m. If the receiver receives the reflected signal from the other building while the direct signal has been blocked, there will be the largest errors higher than 15m. And if the receiver receives the direct and reflected signal at the same time, there might be the errors between 6 and 7m. For the receiver located at the center of the street (P = 0.4-0.5), the multipath errors are evenly distributed around 0 and 6m.

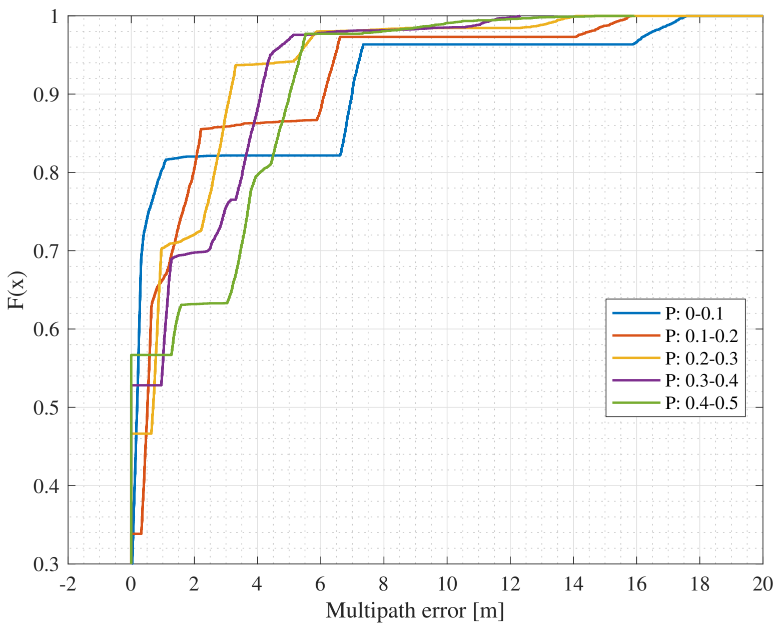

Figure 4.5: The CDF plot for multipath errors with different lateral distances. P is the ratio: distance between receiver to the left building versus street width

Therefore, it is clear that the multipath error distributes evenly when the receiver is in the middle of the street. When the receiver is closer to the left or right building, most of the multipath error will be lower, while there will be some extremely larger error.
Besides the geometry of the street and receiver, the elevation angle of the satellite also has great influence on the multipath error. The elevation angle is the measure used to identify how high up in the sky to look at the satellite. The multipath errors and the corresponding elevation angles are presented in Figure 4.6. This figure is also divided into two subplots to classify the different trends of errors in different elevation angle ranges. From the left subplot of the Figure 4.6, the multipath error has increased as the elevation angle increased from 0 to 45 degree. The trend is opposite in the right subplot of the Figure 4.6 for elevation range within 45 to 80 degree. If the elevation range is higher than 60 degree, the GNSS signal is less likely

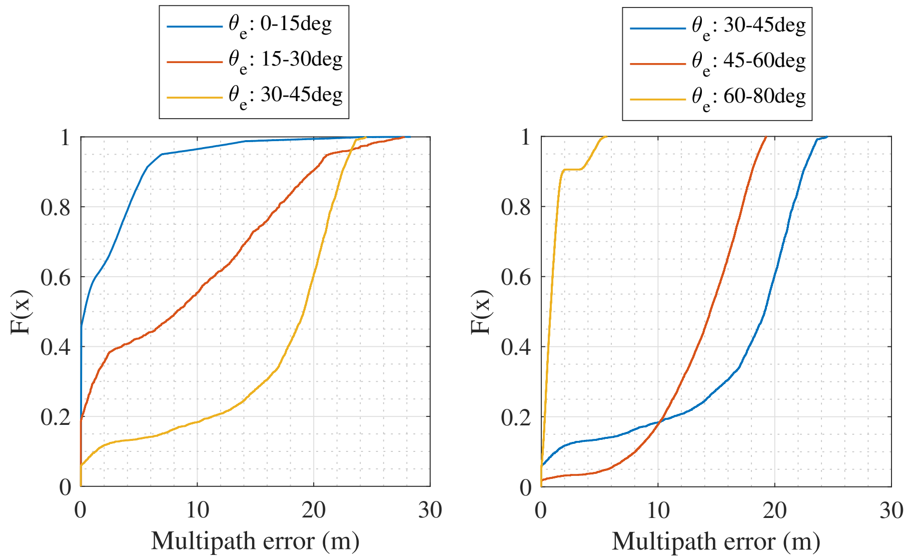

Figure 4.6: The CDF plot for multipath errors with different elevation angles θ_e.

to be blocked and more likely to reach the receiver directly, resulting in a rather low error.
Therefore, as the elevation angle increases from 0 to 80 degree, the multipath error decreases first and then increases. The satellite with the elevation angle within 60-80 degree or 0-15 degree generally has lower multipath error.
Except for that, we also generate the multipath error distributions for different places around the world to see the effect. The multipath error for streets in Gothenburg, Sweden and Shanghai, China are presented in Figure 4.7, which considers the location and typical characteristic of the two places.
In summary, we present the simulation scenarios and parameters in this chapter. The results are analyzed using the performance metrics including estimated position error and multipath error. At last, we compare the GNSS multipath error in different street widths, lateral positions and satellite positions and give the example for multipath error distribution in different cities.

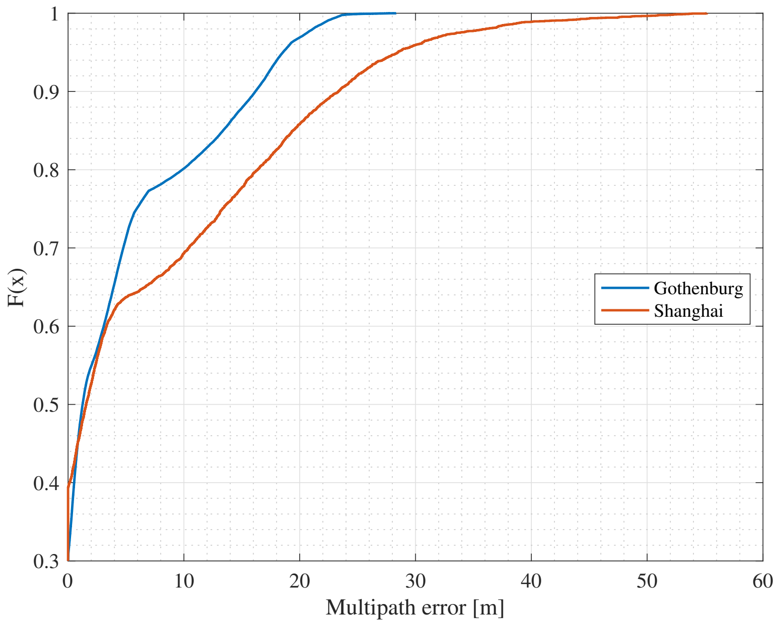

Figure 4.7: The CDF plot for multipath errors for in Gothenburg and Lujia Zui in Shanghai.

5

Conclusion and Outlook

In this chapter, we present the conclusion, limitation and future work of the thesis. At last, the implications of for industrial and academic research of this thesis are presented.

5.1 Conclusion

In this paper, we aim to model the GNSS system error, especially the multipath error with ray tracing method. In the modeling of the multipath error, the latitude and longitude of the location and the street characteristic should be considered as the input.
Therefore, the satellites and urban scenarios are modeled at first. Then, We model the GNSS error including the clock offset error between the satellite and receiver, the tropospheric and ionospheric error, multipath error and receiver measurement error. Most of the GNSS error models can be established by numerical method. While the multipath error is modeled by multipath linear combinations of different signal rays according to the geometric relationship and signal power.
As a result, the present ray tracing model estimates the receiver location by the LS method. The estimation error e_{x} is within 2m, the e_{y} is within 25m, and the e_{z} is within 20m in the present scenario. And the estimation error is the lowest in the direction along the street. Also, by using this ray tracing method for simulation, we found that the multipath error for the satellite which receives signals with multipath components is within 2m, while the multipath error for the NLOS situation reaches for 25m in the given scenario. The estimated multipath error is reasonable compared to other work.
From the perspective of academic area, the effects of various factors on multipath error are analyzed. The street width, the lateral distance of the receiver and the satellite elevation angle all have great influences on the multipath error. This could also help to develop the receiver algorithms to mitigate the multipath error. From the perspective of industrial area, the proposed model could predict the distribution of multipath error with the input of the latitude, longitude of the location and the street characteristic (height and width), which could help with the HIL verification for different cities around the world.

5.2 Future work

For the ray tracing model, there are several limitations and potential future work.

- For the signal properties, the signal polarization and antenna gain are not considered in the model, which could be included in the future.
- For the reception of both direct and reflected signals, we use the signal power as weight to combine the two signals linearly. However in reality, the receiver uses the more complicated methods. This could be implemented in the future work.
- For the position estimation, we use the LS method. More estimation algorithms could be tried such as unweighted least squared method.
- We only consider one reflection. The number of signal reflection as well as the signal penetration could be considered in the later work.
- Due to the limitation of the real data, we did not validate the proposed model with real data, since the data at the pseudorange level have not been found. More research could be done to get some real data (including pseudorange) and the model could be verified.
- The work of combining the error model to the HIL simulation is worthwhile to be conducted.

5.3 Implications for industrial and academic research

In industrial area, the proposed model could help with the multipath error calculation given the location and environment. In academic area, the relationship between the multipath error and the factors of the environment could be analyzed, which could help with the development of GNSS technology.

5.3.1 Industry

In industrial area, this model is proposed mainly for the HIL verification in Volvo. Since there is already the ideal pseudorange signal from the GNSS simulator, we aim to explore the possibility of adding the GNSS error, especially the multipath error, on the ideal GNSS signal. In the HIL verification, cities from different locations around the world need to be simulated and the street characteristics will be significantly different, causing different characteristics of multipath error distribution.

In the proposed model, we use the real satellite position and define the relative position of the street with the longitude, latitude, and altitude information. This means we could simulate the different satellite distributions for different places around world in the HIL verification. What is more, streets with different directions, height ranges and widths could be created and combined in the proposed model, with this the street characteristics for different cities could be reflected, which makes the multipath error in HIL verification more realistic. For example, the multipath error distributions for streets in Gothenburg, Sweden and Shanghai, China are presented in Figure 4.7. Furthermore, the multipath error output by the model proves to be reasonable if we compare it to other research [22] [4]. In the proposed model, the multipath error for the LOS with multipath signal situation are distributed within 2m, as the typical bounded error for this case is less than 2m [22]. Also, Betaille

et al. get the multipath error within 0 to 30m for NLOS situation [4]. And in our model the multipath error for NLOS situation could reach to 25m.
However, the process of adding the generated error on the ideal signal, which is the analog waveform, proves to be a task highly demanding of time and knowledge, which we decide to remain it as future work in this thesis. The proposed model outputs the numerical multipath error at the level of pseudorange for each satellite. The GNSS simulator also generates the ideal pseudorange. However, it outputs the signal as Radio Frequency (RF) signal, which is analog signal. The receiver of this RF signal is also a black box and we could not figure out how it decodes the analog signal and estimates the position. Therefore, adding the generated error on the ideal signal could be another task worth to try in the future.
As a result, the model could help to generate the multipath error according to the location and street characteristic of the city. Also, we have explored the possibility of applying the model on the HIL setup.

5.3.2 Academic

After statistical analysis from the output of the Monte Carlo simulation, three areas including the geometry of the street, the position of the receiver and the satellite position prove to have great influences on the multipath error.
The analysis for the effects of the various factors could give some inspirations for the multipath mitigation in GNSS system. In order to mitigate the multipath error, the elevation angle could be considered during position estimation. For example, after selecting the satellites using dilution of precision and other metrics, we could put more weight on the measurement results of satellites with the highest and lowest elevation angle in the position estimation. Also, if the width of the street is within 50m, the multipath error could be mitigated according to the modeled distribution. If the width of the street is over 50m, some extremely long pseudorange should be considered and removed first. Furthermore, if the vehicle is close to the left or right building, the extremely large path length should be removed.

Reference

[1] Spirent Communications. *What is a GNSS Simulator? Why should you use one for testing?* URL: https://www.nottingham.ac.uk/grace/documents/resources/glossariestutorials/aboutgnsssimulator.pdf. (accessed: 07.10.2010).

[2] Donghyun Kim and Richard B Langley. "GPS ambiguity resolution for long-baseline kinematic applications". In: *GEOIDE Second Annual Conference. Calgary*. 2000, pp. 25–26.

[3] Lawrence Lau and Paul Cross. "Development and testing of a new ray-tracing approach to GNSS carrier-phase multipath modelling". In: *Journal of Geodesy* 81.11 (2007), pp. 713–732.

[4] David Betaille et al. "A new modeling based on urban trenches to improve GNSS positioning quality of service in cities". In: *IEEE Intelligent transportation systems magazine* 5.3 (2013), pp. 59–70.

[5] Yuze Wang, Xin Chen, and Peilin Liu. "Statistical multipath model based on experimental GNSS data in static urban canyon environment". In: *Sensors* 18.4 (2018), p. 1149.

[6] Shiwen Zhang et al. "GNSS multipath detection in urban environment using 3D building model". In: *2018 IEEE/ION Position, Location and Navigation Symposium (PLANS)*. IEEE. 2018, pp. 1053–1058.

[7] John A Klobuchar. "Ionospheric time-delay algorithm for single-frequency GPS users". In: *IEEE Transactions on aerospace and electronic systems* 3 (1987), pp. 325–331.

[8] JP Collins. *Assessment and development of a tropospheric delay model for aircraft users of the global positioning system/by John Paul Collins.* National Library of Canada= Bibliothèque nationale du Canada, Ottawa, 2001.

[9] M Karaim, M Elsheikh, and A Noureldin. "Multifunctional Operation and Application of GPS". In: IntechOpen, 2018. Chap. GNSS Error Sources.

[10] Stefano Bregni. "Clock stability characterization and measurement in telecommunications". In: *IEEE Transactions on instrumentation and measurement* 46.6 (1997), pp. 1284–1294.

[11] Ahmed El-Rabbany. *Introduction to GPS: the global positioning system.* Artech house, 2002.

[12] Karl Rawer. *Wave propagation in the ionosphere.* Vol. 5. Springer Science & Business Media, 2013.

[13] M Karaim. "The long journey of a GPS signal". In: *Inside Signal Processing Newsletter* (2017).

[14] Thomas Hobiger and Norbert Jakowski. “Atmospheric signal propagation”. In: *Springer handbook of global navigation satellite systems*. Springer, 2017, pp. 165–193.

[15] M Kayton. “Global positioning system: signals, measurements, and performance [Book Review]”. In: *IEEE Aerospace and Electronic Systems Magazine* 17.10 (2002), pp. 36–37.

[16] Bradford W Parkinson and James J Spilker. *Progress in astronautics and aeronautics: Global positioning system: Theory and applications*. Vol. 164. Aiaa, 1996.

[17] Mark Pinsky and Samuel Karlin. *An introduction to stochastic modeling*. Academic press, 2010.

[18] Harald T Friis. “A note on a simple transmission formula”. In: *Proceedings of the IRE* 34.5 (1946), pp. 254–256.

[19] David H Staelin. *Electromagnetics and applications*. Massachusetts Institute of Technology, 2011.

[20] Lance de Groot et al. “Precise positioning for automotive with mass market GNSS chipsets”. In: *Proceedings of the 31st International Technical Meeting of The Satellite Division of the Institute of Navigation (ION GNSS+ 2018)*. 2018, pp. 596–610.

[21] Samik Raychaudhuri. “Introduction to monte carlo simulation”. In: *2008 Winter simulation conference*. IEEE. 2008, pp. 91–100.

[22] David F Bétaille, Paul A Cross, and H-J Euler. “Assessment and improvement of the capabilities of a window correlator to model GPS multipath phase errors”. In: *IEEE transactions on aerospace and electronic systems* 42.2 (2006), pp. 705–717.

DEPARTMENT OF SOME SUBJECT OR TECHNOLOGY
CHALMERS UNIVERSITY OF TECHNOLOGY
Gothenburg, Sweden
www.chalmers.se

CHALMERS
UNIVERSITY OF TECHNOLOGY